Mott physics on helical edges of two-dimensional topological insulators

Youhei Yamaji* and Masatoshi Imada
Department of Applied Physics, University of Tokyo, Hongo, Bunkyo-ku, Tokyo 113-8656, Japan and JST-CREST, Hongo, Bunkyo-ku, Tokyo 113-8656, Japan

(Received 13 December 2010; revised manuscript received 8 March 2011; published 20 May 2011)

We study roles of electron correlations on topological insulators or quantum spin Hall insulators on honeycomb lattice with spin-orbit interaction. Accurate variational Monte Carlo calculations with a large number of variational parameters show that the increasing on-site Coulomb interactions cause a strong suppression of the charge Drude weight in the helical-edge metallic states leading to a presumable Mott transition (or strong crossover) from a conventional topological insulator to an edge Mott insulator before a transition to a bulk antiferromagnetic insulator. The intermediate bulk-topological and edge-Mott-insulator phase has a helical spin-liquid character with time-reversal symmetry.

DOI: 10.1103/PhysRevB.83.205122 PACS number(s): 71.27.+a, 71.10.Pm, 72.25.−b, 73.43.−f

I. INTRODUCTION

Recently, spin Hall insulators and its generalization, topological insulators (TIs), have attracted much attention as a new state of matter.[1] A remarkable feature of the newly discovered quantum phase is the Z_2-type topological distinction from other conventional phases as well as the existence of robust gapless edges or surface states concomitant with the bulk insulating gap, which are all protected by the time-reversal symmetry. The edge or surface modes of TI provide us with truly one- or two-dimensional gapless and metallic electronic states.

It has also been proposed that TI may appear in systems under substantial electron correlations such as in $4d$ or $5d$ transition-metal oxides,[2–7] while the interplay of electron correlations with the topological insulator has not been well understood, although the absence of the back scattering protected by the time-reversal symmetry is expected to suppress electron correlation effects.[1,8,9]

In this paper, based on results of calculations obtained from a multivariable variational Monte Carlo (MVMC) methods improved by Tahara and one of the authors,[10] we propose that electron correlation effects introduced by an on-site interaction, namely, a Hubbard U in the Kane-Mele model on the honeycomb lattice, allow a transition or strong crossover from the above TI to an unconventional TI phase characterized by the charge gapped (or nearly insulating) but spin gapless edge excitations with a nonzero spin Drude weight within the same preserved topological nontriviality of the bulk states that are protected by the time-reversal symmetry. This new topological edge Mott insulator (TEMI) phase is stabilized in a region of the intermediate correlation strength sandwiched by a bulk antiferromagnetic insulator (BAFI) with the broken time-reversal symmetry (or bulk Mott insulator) in the larger U region and the simple TI insulator in the weak correlation region.

II. MODEL AND METHOD

We employ a tight-binding Hamiltonian on the two-dimensional honeycomb lattice proposed by Kane and Mele[1] with inclusion of the spin-orbit coupling as complex hopping terms and the on-site Coulomb interaction, and without the Rashba term to study electron correlation effects on the topological insulator. Hereafter we call this simple model the Hubbard-Kane-Mele model and it is defined as

$$\hat{\mathcal{H}} = \hat{\mathcal{H}}_{\rm KM} + U\sum_I \hat{n}_{I\uparrow}\hat{n}_{I\downarrow}, \tag{1}$$

with

$$\hat{\mathcal{H}}_{\rm KM} = -t\sum_{\langle I,J\rangle\sigma}\hat{c}^\dagger_{I\sigma}\hat{c}_{J\sigma} + it_2\sum_{\langle\langle I,J\rangle\rangle\alpha\beta}\nu_{ij}\hat{c}^\dagger_{I\alpha}[\sigma_z]_{\alpha\beta}\hat{c}_{J\beta}, \tag{2}$$

where $\hat{\mathcal{H}}_{\rm KM}$ is the Kane-Mele Hamiltonian, t (t_2) is the nearest-neighbor (next-nearest-neighbor) hopping, and U is the on-site Hubbard interaction. Here we define $\nu_{ij} = \vec{d}_i \times \vec{d}_j / |\vec{d}_i \times \vec{d}_j|$, and $I = (i,a)$ $(a = A,B)$ (see Fig. 1). We perform unrestricted Hartree-Fock (UHF) calculations as well as MVMC calculations by optimizing a large number of variational parameters.

In the UHF calculation, we decouple the U term as

$$\begin{aligned}\hat{n}_{I\uparrow}\hat{n}_{I\downarrow} \simeq\ & \langle\hat{n}_{I\uparrow}\rangle\hat{n}_{I\downarrow} + \langle\hat{n}_{I\downarrow}\rangle\hat{n}_{I\uparrow} - \langle\hat{n}_{I\uparrow}\rangle\langle\hat{n}_{I\downarrow}\rangle - \langle\hat{c}^\dagger_{I\uparrow}\hat{c}_{I\downarrow}\rangle\hat{c}^\dagger_{I\downarrow}\hat{c}_{I\uparrow} \\ & - \langle\hat{c}^\dagger_{I\downarrow}\hat{c}_{I\uparrow}\rangle\hat{c}^\dagger_{I\uparrow}\hat{c}_{I\downarrow} + \langle\hat{c}^\dagger_{I\uparrow}\hat{c}_{I\downarrow}\rangle\langle\hat{c}^\dagger_{I\downarrow}\hat{c}_{I\uparrow}\rangle.\end{aligned} \tag{3}$$

For the MVMC calculations, we employ a variational wave function[10] defined as

$$|\psi\rangle = \mathcal{P}_{\rm G}\mathcal{P}_{\rm J}|\phi_{\rm pair}\rangle, \tag{4}$$

where $\mathcal{P}_{\rm G}$ is the Gutzwiller factor defined by

$$\mathcal{P}_{\rm G} = \exp\left[-\sum_I g_I\hat{n}_{I\uparrow}\hat{n}_{I\downarrow}\right], \tag{5}$$

and $\mathcal{P}_{\rm J}$ is the Jastrow factor defined by

$$\mathcal{P}_{\rm J} = \exp\left[-\frac{1}{2}\sum_{I,J} v_{IJ}(\hat{n}_{I\uparrow}+\hat{n}_{I\downarrow})(\hat{n}_{J\uparrow}+\hat{n}_{J\downarrow})\right], \tag{6}$$

with the spatially dependent variational parameters g_I and v_{IJ}. We impose the Gutzwiller factor on all the sites, whereas introduce the Jastrow factor only along the zigzag edges. The

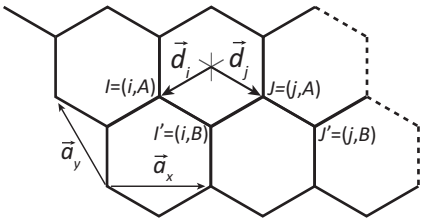

FIG. 1. Honeycomb lattice on which the Hubbard-Kane-Mele model is defined.

one-body part $|\phi_{\rm pair}\rangle$ is a generalized pairing wave function defined as

$$|\phi_{\rm pair}\rangle = \left[\sum_{i,j=1}^{N_{\rm s}} f_{ij} c_{i\uparrow}^{\dagger} c_{j\downarrow}^{\dagger}\right]^{N/2} |0\rangle \tag{7}$$

with f_{ij} being the complex variational parameters. In this study, we allow f_{ij} to have two-sublattice ($2 \times L_y$-sublattice) structure or equivalently we have $2 \times 2 \times N_{\rm s}$ ($2 \times L_y \times 2 \times L_y \times L_x$) variational parameters for the torus (cylinder). All the variational parameters are simultaneously optimized by using the stochastic reconfiguration method[10,11] generalized for complex variables. The accuracy of this method has been proven in a number of benchmarks.[10,12] In addition, the MVMC does not have so-called sign problems.

Charge and spin Drude weights are calculated by introducing vector potentials as the Peierls factors,

$$t_{IJ\sigma} \to t_{IJ\sigma} \exp[i\vec{A}_\sigma \cdot \vec{r}_{IJ}], \tag{8}$$

where $\vec{r}_I = n_I \vec{a}_x + m_I \vec{a}_y$ and $\vec{r}_{IJ} = \vec{r}_I - \vec{r}_J$. Here n_I and m_J are integers, and lattice vectors are $\vec{a}_x$ and $\vec{a}_y$ (see Fig. 1). From this Peierls factor, the charge and spin Drude weights, $D_{\rm c}$ and $D_{\rm s}$, respectively, are calculated from the energy stiffness,[13]

$$D_{\rm c} = \frac{1}{2}\frac{d^2 E(\vec{A}_\uparrow, \vec{A}_\downarrow)}{d|\vec{A}|^2}\bigg|_{\vec{A}_\uparrow = \vec{A}_\downarrow}, \tag{9}$$

and

$$D_{\rm s} = \frac{1}{2}\frac{d^2 E(\vec{A}_\uparrow, \vec{A}_\downarrow)}{d|\vec{A}|^2}\bigg|_{\vec{A}_\uparrow = -\vec{A}_\downarrow}, \tag{10}$$

where $E = \langle\psi|\hat{\mathcal{H}}|\psi\rangle/\langle\psi|\psi\rangle$ is the total energy. To clarify the edge state, we employ a cylinder with sizes $N_s = L_x \times L_y \times 2$, for the honeycomb lattice with two sites on a unit cell and the periodic (free) boundary conditions in the x (y) directions. We have confirmed that the employed width L_y is large enough to make isolated two edges at the two free boundaries at $y = 0$ and $y = L_y$. For the bulk properties we employ the torus, where the boundary is periodic for all directions.

III. RESULTS

A. Bulk phase diagram

The ground-state phase diagram of the bulk is shown in Fig. 2 for the Hubbard-Kane-Mele model on the torus. Our MVMC results show the antiferromagnetic transition at $U = U_{\rm c}^{\rm AF} \sim 7t$ for $t_2 = 0.1t$. Below $U \sim 7t$, the bulk stays

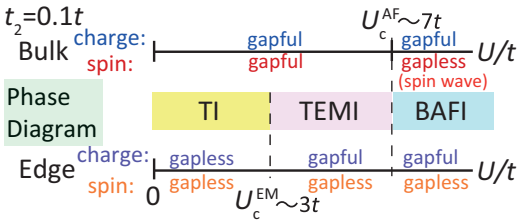

FIG. 2. (Color online) Phase diagram of the Hubbard-Kane-Mele model proposed based on MVMC containing three phases for $t_2 = 0.1t$. The bulk on the torus shows a phase transition from TI to the bulk antiferromagnetic insulator (BAFI) at $U/t \sim 7$. On the cylinder, the edge shows insulating behaviors for $3t \lesssim U$. The intermediate TEMI phase or region is a possible gapless spin liquid at the edges.

as a topological insulator and the peak height of the magnetic structure factor defined by

$$S_{\rm AF}(\vec{q}) = \frac{1}{3N_s}\sum_{I,J} e^{i\vec{q}\cdot\vec{r}_{ij}} \lambda_I \lambda_J \hat{\vec{S}}_I \cdot \hat{\vec{S}}_J, \tag{11}$$

for the spin-1/2 operator $\hat{\vec{S}}_I$ scales to a size-independent constant after the size extrapolation, in contrast to the Bragg peak height proportional to $N_s = L_x \times L_y \times 2$ observed in BAFI, as is shown in Fig. 3. Here we have shown the peak values, which appear at the wave number $q = 0$ and for the staggered modes within the unit cell, namely $\lambda_I = +1(-1)$ for $I = (i,A)$ [$I = (i,B)$]. The MVMC calculation gives the critical value of U for $t_2 \neq 0$ larger than that for $t_2 = 0$. These results for the bulk are qualitatively consistent with an auxiliary-field quantum Monte Carlo simulation for $t_2 = 0$, which shows $U_{\rm c}^{\rm AF} = 4.3t$,[14] and a slave-rotor mean-field result for $t_2 \neq 0$,[15] although the conclusion of Ref. 15 for the edge is different from ours.

Here the magnetic moments in the BAFI phase align in the xy plane. This fact conforms with the UHF results and the effective Hamiltonian at the strong-coupling limit (see Ref. 15); the second-order perturbation of the second-neighbor

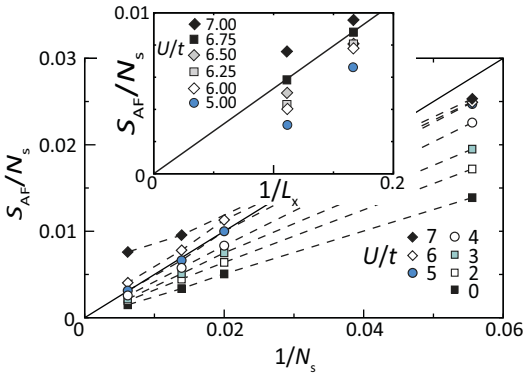

FIG. 3. (Color online) $1/N_s$ dependences of $S_{\rm AF}(\vec{q} = \vec{0})$ on the torus, where $L_x = L_y$. The inset shows the same quantity vs $1/\sqrt{N_s/2}$ ($=1/L_x$). We note that S_{AF}/N_s may be scaled linearly with $1/N_s$ as $1/N_s \to 0$ in the disordered phase (see Fig. 3), whereas it should be scaled linearly with $1/L_x$ with a nonzero offset in the ordered phase consistent with the spin-wave theory (see the inset). These scalings suggest that the phase transition occurs between $U = 6.75t$ and $U = 7t$.

hopping it_2 yields the second-neighbor exchange coupling as $J_2[\hat{S}_i^z\hat{S}_j^z - \hat{S}_i^x\hat{S}_j^x - \hat{S}_i^y\hat{S}_j^y]$, where $J_2 = 4t_2^2/U$. In the xy plane, J_2 gives the ferromagnetic coupling and stabilizes the BAFI moment within this plane. The nonzero magnetic moment within the xy plane always opens a gap at the edge modes, although an infinitesimal magnetic moment along the z axis does not open a gap.

B. Edge transport

We show MVMC results for the Drude weights for the Hubbard-Kane-Mele model on the cylindrical geometry with two zigzag edges along the x direction. If we introduce spin-dependent vector potentials, $\vec{A}_\sigma = \sigma\vec{A}$, we obtain the Drude weight for the spin channel,[16] namely the spin Drude weight. The topologically nontrivial phase is probed by directly calculating the Z_2 topological number as is proposed by Lee and Ryu.[17] However, it requires much more computational cost. Alternatively and equivalently, the gapless edge probed by the Drude weight concomitant with the gapped bulk state on the cylinder ensures the existence of the topologically nontrivial phase.[1]

In Fig. 4, we compare the results for charge and spin Drude weights by MVMC with those of the UHF approximation. Here we only retain self-consistent UHF solutions without xy components of magnetic moments when we calculate the Drude weights by using UHF. The data for $15 \times 5 \times 2$ well represent the thermodynamic limit of the nonmagnetic self-consistent UHF solution without the xy component of the magnetic moments. We see consistent suppression (enhancement) of the charge (spin) Drude weight $D_c(D_s)$ arising from the increasing on-site Coulomb interaction U. Moreover, the suppression (enhancement) of $D_c(D_s)$ has nearly linear dependences on U/t.

Now we estimate the transition or crossover point where D_c becomes vanishing. The strong suppression of D_c is already clear from our finite-size study, which proves the emergence of such a qualitatively new region with suppressed D_c, namely edge insulating behavior. However, within the present numerical accessibility, it is not easy to make size extrapolation to pin down the phase boundary. To make the best estimate of the thermodynamic limit, we utilize the UHF result as a reference, because the thermodynamic limit in the UHF can be easily estimated. Although the MVMC ground states and the nonmagnetic UHF solutions seem to show

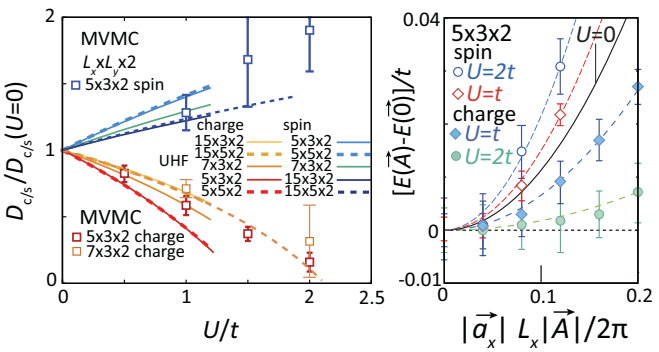

FIG. 4. (Color online) Left panel: U dependence of renormalized Drude weights. Right panel: vector potential dependences of total energy E for $L_x = 5$, $L_y = 3$.

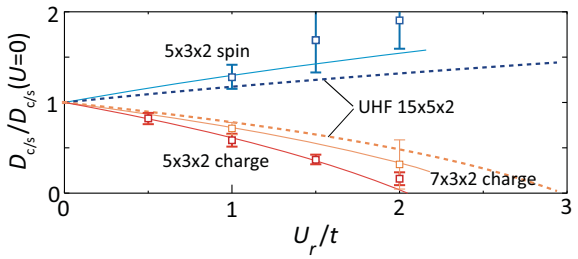

FIG. 5. (Color online) Renormalized $D_c(U_r/t)/D_c(0)$ of the UHF and MVMC. The solid curves for the UHF data scales identically with the MVMC data for the same sizes when we employ the renormalized interaction U_r.

different U dependence of the Drude weights, the renormalized dependences of $D_c(U_r/t)/D_c(0)$ vs U_r/t with $U_r = U$ for MVMC and $U_r \simeq 1.4 \times U$ for UHF remarkably make all of them universal. This fact indicates that our estimate for the phase boundary by the MVMC with the help of the finite-size correction extracted from the UHF as is shown in Fig. 5 is close to the thermodynamic limit. The MVMC results support a transition or strong crossover on the edge from the TI to a charge gapped (or nearly insulating) phase (TEMI) around $U_c^{\mathrm{EM}} \sim 3t$ in the thermodynamic limit.[18]

The suppression and enhancement in the Drude weights are naturally accounted for by focusing on the spin and charge pumping caused by the vector potentials. The spin-independent (spin-dependent) vector potential causes the spin (charge) pumping along the zigzag edges,[1] which is nothing but the celebrated quantum spin Hall effects in the Kane-Mele model. Without the Rashba term, which mixes the spin-up and -down components, the spin-independent vector potential causes a spin pumping of the z components. Here we note that the small amount of spin accumulation of the z component does not induce a gap opening at the edge modes. Even when we introduce the Hubbard U, the signature of the spin pumping due to the small amplitude of the spin-independent vector potential remains as is typically shown in Fig. 6 and continues even beyond $U/t \sim 3$ (not shown).

The spin pumping generates spin polarization along the z axis at the edges, which helps electrons to reduce the cost of the Hubbard U. Contrarily, the charge pumping forces to

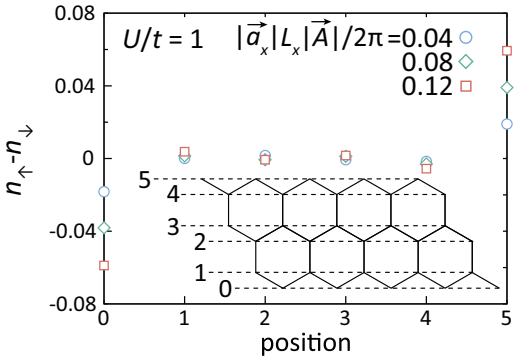

FIG. 6. (Color online) Position dependence along the cylinder width of averaged spin polarizations $n_\uparrow - n_\downarrow$ due to vector potentials $\vec{A}_\sigma$, for $U/t = 1$, $L_x = 5$, and $L_y = 3$. Inset shows the numbering of the position along the cylinder width.

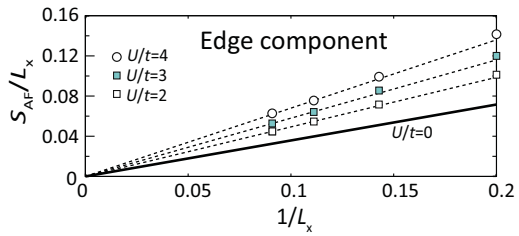

FIG. 7. (Color online) $1/L_x$ dependences of edge components in $S_{\rm AF}(\vec{q}=\vec{0})$ on the cylinder with $L_y=3$. Here we restrict the summation for I,J in Eq. (11) within the single edge, namely, $i=0,1,\ldots,L_x-1$, and $j=0$. Error bars are all within the symbol sizes.

increase the double occupation at the edges resulting in the cost of U. Therefore the energy increase with increasing vector potential (namely the stiffness or the Drude weight as the quadratic coefficients) decreases (increases) compared with E of the noninteracting system. Such spin-charge separated Drude weights appear even in the restricted Hartree-Fock calculation, which does not allow the magnetic moments within the xy plane.

C. Edge phase diagram

Based on the calculated spin and charge Drude weights, we show the edge phase diagram in Fig. 2. It supports a metal-insulator transition at the edge at $U=U_{\rm c}^{\rm EM}\sim 3t$, where the edge and bulk still continue to be paramagnetic beyond it. As is evident in the edge component in the $S_{\rm AF}(\vec{q}=\vec{0})$ shown in Fig. 7, there is no edge magnetism at least up to $U=4t$. In contrast, the coherent edge spin transport is enhanced by increasing U.

The low-energy effective model for the interacting edge modes, namely, the helical Tomonaga-Luttinger liquid, does not include the back scattering and umklapp channels,[8,9] which are, in general, essential for the formation of insulating phases. However, for $t_2=0.1t$ and $U\sim 3t$, the amplitude of the bulk gap, which limits the energy scale to justify the treatment by the topological band insulator, becomes comparable with U. Then, the helical Tomonaga-Luttinger liquid will fail to capture this Mott insulating behavior of the edge modes. In fact, a large Coulomb repulsion ($U\gg t$, t_2) inevitably prohibits coherent propagations of electrons. In reality, it actually results in gapped charge excitations for $t_2=0.1t$ and $U_{\rm c}^{\rm EM}(\sim 3t)\leqslant U\leqslant U_{\rm c}^{\rm AF}(\sim 7t)$ with gapless spin excitations at the edge for the Hubbard-Kane-Mele model.

D. Whole phase diagram

As we see in Fig. 2, through the U variation, the bulk state is always insulating (charge gapped) if the spin-orbit interaction is nonzero while it has a spin gapless excitation exclusively in the conventional bulk Mott insulator or BAFI phase at the largest U region. However, the edge state is always characterized by the gapless spin excitations while the charge excitation is gapless only in the lowest U region of the TI phase. Then we find the intermediate phase, TEMI, where the bulk excitations are gapped in both spin and charge channels, while in the edge state the charge excitation is gapped (insulating) and the spin excitation is gapless with a spin-liquid behavior. We note that this general phase diagram with three phases contained may be universal also in three-dimensional systems except for the additional possibility that, depending on the lattice geometry, the spin liquid in the TEMI phase could be replaced with the magnetic symmetry breaking such as the antiferromagnetic order at the edge (surface).[6]

IV. DISCUSSION

A possible interpretation of the TEMI phase is a fermionic spinon liquid under the fractionalized electrons in the slave-rotor approximation proposed by Young *et al.*,[2] Pesin and Balents,[3] and Rachel and Le Hur.[15] However, in two-dimensional systems, it is believed that the fractionalization of electrons cannot happen due to gauge fluctuations,[3,15] which invalidates the starting point of Ref. 15 and the description by the electrons become adequate. Our present approach starts from this electron and accurately takes into account the correlation effects beyond the mean-field treatment of the electron's single-particle picture. It is a nonperturbative calculation and is based on the electron wave functions consisting of linear combination of a huge number of Slater determinants, which include the resonant-valence-bond states,[19] and can reproduce accurate results comparable with unbiased numerical methods.[10,20] In addition, the one-dimensional spin-charge separation in the simple Hubbard chain is characterized by the spin/charge excitations as bosonic collective modes of the Tomonaga-Luttinger liquid.[21,22] In the present spin liquid on the edges,[23] it is also likely to have gapped charge and gapless spin bosonic collective density modes leading to the helical Tomonaga-Luttinger liquid,[8,9] distinct from the chiral Tomonaga-Luttinger liquid[22] in the quantum Hall phase. It is intriguing whether this spin liquid retains its helical nature. The present numerical accuracy does not allow us to reach a definite conclusion. However, it is known that the change in the topological index requires the closing of the bulk charge gap,[1,24] which is apparently not the case around $U/t=3$. It indicates that the topologically nontrivial bulk phase is retained and it requires the helical nature in the edge.

The conventional TI in the cylinder geometry is characterized by the nonzero diagonal charge (spin) conductivities denoted by $\sigma_{ccxx}\neq 0$ ($\sigma_{ssxx}\neq 0$) and nonzero spin-charge transverse conductivity denoted by $\sigma_{csxy}=\sigma_{scxy}\neq 0$ and $\sigma_{csyx}=\sigma_{scyx}\neq 0$, where all are solely from the edge contributions. Other spin-charge off-diagonal elements are zero. On the other hand, the present TEMI with the gapped charge and gapless spin liquid edges keeps $\sigma_{ssxx}\neq 0$ again contributed only from the edge, whereas all the other elements including σ_{ccxx}, $\sigma_{csxy}=\sigma_{scxy}$ and $\sigma_{csyx}=\sigma_{scyx}$ vanish. The Onsager reciprocal relation of course always holds. In the both TI and TEMI phases, all the bulk conductivities vanish, while in the bulk Mott insulator (or BAFI) phase, the bulk and edge spin conductivities may remain nonzero while all the other linear responses involving the charge part vanish irrespective of bulk or edge.

Recently we became aware of two related works.[25,26] A model with U retained only at the edge sites employed in Ref. 25 could cause a substantial difference from the present realistic choice. However, irrespective of this difference, quantum Monte Carlo simulations reported in Ref. 25

also show the suppression of coherent charge transports. Reference 26 employs only even numbers for L_x, where the ground-state degeneracy in the open shell condition always remains and requires careful treatment.

V. SUMMARY

Our present variational Monte Carlo calculations show that the local electron correlation U of the Hubbard-Kane-Mele model on the honeycomb lattice drives a strong crossover or a quantum phase transition within the topologically nontrivial phase. The transition appears to separate an edge metallic TI phase at lower U from TEMI phase with charge gapped and spin gapless (spin liquid) edges at larger U, where a bulk charge-spin gap is always retained through these two topological phases. Namely, the larger U phase is characterized by a vanishing charge Drude weight together with a nonzero and large spin Drude weight on the edge in contrast to the both large charge and spin Drude weights in the lower U phase. With further increase of U, this TEMI phase undergoes a transition into the BAFI phase with time-reversal symmetry breaking.

In a naive interpretation, one may find a Berezinskii-Kosterlitz-Thouless-type transition in the charge sector at the transition between the TI and TEMI, where the charge degrees of freedom gains a mass term of the equivalent sine-Gordon model in the TEMI. On the other hand, a helical type of Tomonaga-Luttinger liquid continues in the spin sector even in the TEMI phase. However, the helical nature requires careful consideration and the real nature of spin liquid in the TEMI phase deserves further clarification. In fact, essentially the same bulk topological insulators may have a variety of different types of edge or surface states depending on how the electron correlation effects are switched on. Other quantum states unexplored in the conventional materials may emerge in this circumstance. Efforts to reveal new states will open an avenue in the research of physics of topological insulators.

ACKNOWLEDGMENTS

Y.Y. thanks Daisuke Tahara for sharing his VMC code for real f_{ij}. He also thanks Takahiro Misawa, Hiroshi Shinaoka, and Moyuru Kurita for useful discussions. We thank financial support from Computational Materials Science Initiative, and MEXT Japan under Grants No. 22104010 and No. 22340090. We would like to thank Computational Materials Science Initiative for support.

*yamaji@solis.t.u-tokyo.ac.jp

[1] C. L. Kane and E. J. Mele, Phys. Rev. Lett. **95**, 146802 (2005); L. Fu and C. L. Kane, Phys. Rev. B **74**, 195312 (2006); L. Fu, C. L. Kane, and E. J. Mele, Phys. Rev. Lett. **98**, 106803 (2007).
[2] M. W. Young, S.-S. Lee, and C. Kallin, Phys. Rev. B **78**, 125316 (2008).
[3] D. Pesin and L. Balents, Nat. Phys. **6**, 376 (2010).
[4] B.-J. Yang and Y. B. Kim, Phys. Rev. B **82**, 085111 (2010).
[5] X. Wang *et al.*, e-print arXiv:1007.0016 (to be published).
[6] A. Shitade, H. Katsura, J. Kunes, X. L. Qi, S. C. Zhang, and N. Nagaosa, Phys. Rev. Lett. **102**, 256403 (2009).
[7] C. N. Varney, K. Sun, M. Rigol, and V. Galitski, Phys. Rev. B **82**, 115125 (2010).
[8] C. Wu, B. A. Bernevig, and S. C. Zhang, Phys. Rev. Lett. **96**, 106401 (2006).
[9] C. Xu and J. E. Moore, Phys. Rev. B **73**, 045322 (2006).
[10] D. Tahara and M. Imada, J. Phys. Soc. Jpn. **77**, 114701 (2008).
[11] S. Sorella, Phys. Rev. B **64**, 024512 (2001).
[12] M. Imada and T. Miyake, J. Phys. Soc. Jpn. **79**, 112001 (2010).
[13] W. Kohn, Phys. Rev. **133**, A171 (1964).
[14] Z. Y. Meng *et al.*, Nature (London) **464**, 847 (2010).
[15] S. Rachel and K. Le Hur, Phys. Rev. B **82**, 075106 (2010).
[16] P. Kopietz, Phys. Rev. B **57**, 7829 (1998).
[17] S.-S. Lee and S. Ryu, Phys. Rev. Lett. **100**, 186807 (2008).
[18] This TEMI phase has an apparent similarity to the spin liquids in Ref. 14, but is qualitatively distinct from the bulk phase with a spin gap identified at $t_2 = 0$ in Ref. 14. In addition, if the TEMI phase is a real quantum phase, it should be different from the spin liquid claimed to exist only in three-dimensional models in Ref. 15.
[19] S. Liang, B. Doucot, and P. W. Anderson, Phys. Rev. Lett. **61**, 365 (1988).
[20] D. Tahara and M. Imada, J. Phys. Soc. Jpn. **77**, 093703 (2008).
[21] H. J. Schulz, Phys. Rev. Lett. **64**, 2831 (1990).
[22] J. Voit, Rep. Prog. Phys. **58**, 977 (1995).
[23] Our present results support that the edge modes remain helical even in the presence of the Hubbard U. If the edge spin Drude weights continue to arise from the gapless edge modes, the spin pumping due to the spin independent vector potentials (see Fig. 6) is a strong indication of the helical edge modes.
[24] S. Murakami and S. I. Kuga, Phys. Rev. B **78**, 165313 (2008).
[25] M. Hohenadler, T. C. Lang, and F. F. Assaad, Phys. Rev. Lett. **106**, 100403 (2011).
[26] D. Zheng, C. Wu, and G.-M. Zhang, e-print arXiv:1011.5858 (to be published).